Detonation development in PRF/air mixtures under engine-relevant conditions

Hsu Chew Lee [a], Peng Dai [a,*], Zheng Chen [b], Xiaohua Gan [a]

[a] *Department of Mechanics and Aerospace Engineering, Southern University of Science and Technology, Shenzhen 518055, China*

[b] *SKLTCS, CAPT, BIC-ESAT, College of Engineering, Peking University, Beijing 100871, China*

Abstract

The development of advanced boosted internal combustion engines (ICEs) is constrained by super-knock which is closely associated with end gas autoignition and detonation development. The present study numerically investigates the transient autoignition and detonation development processes under engine-relevant conditions for primary reference fuel (PRF) consisting of n-heptane and iso-octane. The effects of PRF composition are systematically examined. By considering the transient local sound speed rather than its initial value, a new non-dimensional parameter is proposed to assess the transient chemical-acoustic interaction and to quantify the autoignition modes. Two detonation sub-modes, normal and over-driven detonation, are identified and the corresponding mechanisms are interpreted. For the over-driven detonation, there exist two developing regimes with weak/strong chemical-acoustic coupling and slow/rapid pressure enhancement. It is found that the maximum pressure caused by autoignition decreases with the blending ratio of iso-octane, mainly due to the increase in excitation time. Besides, the strongest detonation induced by hot spot usually occurs within the over-driven detonation sub-regime. Its condition can be well quantified by the new non-dimensional parameter proposed in work and its strength is determined by the ratio of hot spot acoustic time to excitation time. The deviation of transient autoignition front propagation from prediction based on homogenous ignition is mainly attributed to the non-uniform compression effect caused by gradually enhanced pressure wave, while the influence of heat conduction and mass diffusion is negligible. The initial expansion stage dominating the induction period of local autoignition is greatly influenced by the compression of pressure wave. Therefore, the continuously enhanced pressure wave non-uniformly changes the local ignition delay (i.e. reduces its spatial gradient) within the hot spot and thereby accelerates the autoignition front propagation. The relationship among the parameters quantifying the detonation propensity is assessed and interpreted. The present study provides helpful understanding of detonation development under engine conditions.

Keywords: Detonation development; Autoignition; Hot spot; PRF; Pressure wave

---

*Corresponding author.

1. Introduction

Currently, the advancement of boosted spark ignition engine (SIE) technologies is constrained by a newly discovered phenomenon, super-knock, which is characterized by its random occurrence and extremely destructive pressure oscillation [1-3]. Super-knock is commonly attributed to detonation development which was demonstrated to be caused by spontaneous ignition of hot spot and mutual coupling between local autoignition and pressure wave [2-5]. However, the quantitative conditions for detonation occurrence in SIEs are still not fully understood. Since gasoline used in SIEs consists of hundreds of species and its physical/chemical properties can hardly be represented by one single component, surrogate fuel models such as Primary Reference Fuel (PRF) [6, 7] and Toluene Reference Fuel (TRF) [8, 9] are widely used. Unfortunately, there is currently a lack of studies on detonation and super-knock for surrogate fuel blends, and it is still unclear how the composition of these fuels affects the different autoignition modes. Therefore, a comprehensive understanding of autoignition and detonation development in surrogate fuels under engine-relevant conditions is of both fundamental and practical interest.

In order to quantify the detonation propensity induced by a hot spot, Bradley and co-workers [10, 11] proposed the so-called detonation peninsula described by two parameters: the normalized temperature gradient (ξ) and the ratio of acoustic time to excitation time (ε). The detonation development can be interpreted using the reactivity gradient theory [12, 13] and shock wave amplification by coherent energy release (SWACER) mechanism [14]. This detonation peninsula was widely utilized in the studies on engine knock [2, 5, 15-21]. However, recent studies [8, 9, 22, 23] showed that the detonation regime in the ξ-ε diagram quantitatively depends on thermodynamic conditions and mixture composition. Specifically, it was found in our previous studies [19, 22, 23] that the transient autoignition front propagation speed greatly deviates from the prediction by parameter ξ and therefore leads to different autoignition modes with varying mixture conditions. The relevant mechanism, however, is still not well known. Besides, Pan et al. [18] examined the detonation formation and termination outside the hot spot and found that the mixture reactivity therein also plays an important role in detonation development. Luong et al. [24, 25] examined the effects of temperature fluctuations and turbulence on the detonation development and engine knock. They proposed several statistical parameters including the volume-averaged ξ in predicting knock intensity. Recently, we have investigated the autoignition in a confined space and identified different autoignition modes respectively from the hot spot and the end wall caused by pressure/shock wave reflection [26].

Most of the previous studies on autoignition and detonation development only considered single fuel, and there are only a few studies on fuel blends [8, 9, 11, 17]. Zaccardi and co-workers [8, 9] investigated the autoignition modes induced by a hot spot for TRF surrogate using Large Eddy Simulations (LES), and identified the detonation regimes in ξ-ε diagram under different thermodynamic conditions. Lechner et al. [17] found that ξ-ε diagram can qualitatively reproduce the knock propensity of methane, biogas, propane and syngas blends, which increases with the addition of higher hydrocarbons. However, the quantitative variation of detonation propensity with the composition of surrogate model and the corresponding key mechanisms have not been fully investigated before. This motivates the present study, which considers PRF blends consisting of n-heptane and iso-octane. The objectives of this study are three-fold: (1) to assess the impact of PRF composition on the autoignition and detonation development induced by a hot spot; (2) to interpret the mechanism causing the deviation of the transient autoignition front propagation from 0-D prediction; and (3) to quantitatively determine the critical conditions of typical autoignition modes for various PRF compositions.

2. Numerical model and specifications

Here we consider PRF consisting of n-heptane and iso-octane. The blending ratio, c, defined as the molar fraction of iso-octane, changes from 0 (pure n-heptane) to 1 (pure iso-octane). The recently developed skeletal PRF model [7] consisting of 171 species and 861 reactions is used in simulations.

We study the transient autoignition process initiated by a hot spot in a stoichiometric PRF/air mixture. This mixture is inside an adiabatic, closed, spherical chamber and the hot spot is at the center. The turbulence is not considered. It is noted that turbulence might significantly influence the autoignition process when the time/length scales of physical-chemical processes are comparable with those of turbulence [21, 24]. This deserves further investigation in future work. An ideal and simplified model is used here to isolate the major mechanisms of detonation development and to quantify the critical conditions for various autoignition modes (for example, the effects of wall cooling [27] and normal flame propagation [28, 29] are not considered here). Therefore, the condition here is not fully representative to the real engines. Due to spherical symmetry, 1-D simulations are conducted along the radius of the spherical chamber. The hot spot is at the left end of the computation domain and characterized by linear temperature distribution with negative gradient:

$$T_i(r)=\begin{cases} T_{i,0}+(r-r_0)(dT/dr)_i & (r\le r_0) \\ T_{i,0}=1000\ \mathrm{K} & (r_0<r\le R_w) \end{cases} \quad (1)$$

where r is the radial spatial coordinate; r_0 is the hot spot radius ranging from 1 to 8 mm (i.e., r_0=1, 2, 3.5, 5 and 8 mm); R_w=4 cm is the radius of the spherical

chamber, noting that the autoignition process will be complicated by the pressure/shock wave reflection at end wall when the domain is small enough (e.g. $R_w \leqslant$ 2 cm) [26]; $(dT/dr)_i$ is the specified initial temperature gradient of the hot spot which ranges from -0.1 to -4 K/mm, with enough (i.e. more than 20) points chosen to fully resolve the variation trend of autoignition characteristics (e.g., see Fig. 5 as shown later); and $T_{i,0}$=1000 K is the initial temperature outside the hot spot, which is chosen to exclude the influence of low-temperate chemistry [19, 20, 23] and to facilitate direct comparison with the results in the literature. The PRF/air mixture in the chamber is initially uniform and static at P_0=40 atm. Four PRF compositions are considered: PRF0 (pure n-heptane), PRF50 (c=0.5), PRF80 (c=0.8) and PRF100 (pure iso-octane). The Chapman-Jouguet detonation wave speed is $D_{C\text{-}J}$=1845.6 (1846.3) m/s and the von-Neumann spike pressure is $P_{v\text{-}N}$=237.7 (238.4) atm for PRF0 (PRF100).

The transient autoignition process is simulated using the in-house code A-SURF [19, 30, 31]. The conservation equations for 1-D, compressible, adiabatic, multi-component, reactive flow are solved using the finite volume method. The mixture-averaged model is employed to compute species diffusion velocity. A multi-level, dynamically adaptive mesh algorithm is used to resolve the reaction zone, pressure wave, shock wave and detonation wave, which are covered by the finest mesh of 1.56 μm. The corresponding time step is 0.312 ns. The details on governing equations, numerical scheme and code validation can be found in Refs. [19, 20, 22]. It is noted that the ideal-gas equation of state is used here and therefore the obtained condition in the region of extremely high pressure spike of detonation wave can only be approximations of the real situation. Grid convergence is ensured and demonstrated in the Supplementary Material.

3. Results and discussion

Figure 1 shows the ignition delay time (τ, defined as the time for maximum heat release rate) and excitation time (τ_e, defined as the time interval between 5% and maximum heat release rate [11]) at different PRF blending ratios. The results are obtained by simulating the constant-volume homogeneous ignition process. Figure 1 also shows the critical temperature gradient [11], $(dT/dr)_c$, at which the theoretical autoignition front propagation speed, u_a^0, equals to the initial sound speed, a^0:

$$(dT/dr)_c = \left(a^0 \left(d\tau/dT_0\right)\right)^{-1} \tag{2}$$

Generally both τ_e and τ become larger at higher PRF blending ratio, c. When $c \leq 0.2$, τ is insensitive to c. However, τ increases rapidly with c for $c \geq 0.2$. The magnitude of $(dT/dr)_c$ decreases greatly with c and can be reduced by almost 80% through iso-octane blending. This indicates that the same thermal hot spot might induce different autoignition modes for different PRF blends. Corresponding results at varying T_0 are illustrated in the Supplementary Material (see Fig. S2) and similar trends to those shown in Fig. 1 are observed. The 0-D and 1-D ignition processes are also simulated by using a reduced PRF mechanism consisting of 73 species and 296 reactions [6]. The corresponding results are found to be similar to those shown in this paper though some quantitative discrepancies exist (see Figs. S3 and S6 of the Supplementary Material).

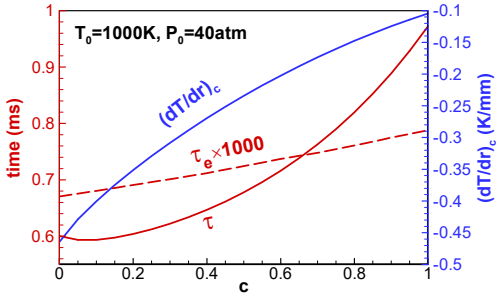

Fig. 1 Change of homogeneous ignition delay time, excitation time and critical temperature gradient with the PRF blending ratio at T_0=1000 K and P_0 = 40 atm.

According to Gu et al. [11], the normalized temperature gradient of the hot spot, ξ, is defined as

$$\xi = (dT/dr)_i \big/ (dT/dr)_{c,r_0/2} \tag{3}$$

where $(dT/dr)_{c,r0/2}$ denotes the critical temperature gradient calculated at $r=r_0/2$ in order to represent the average condition within the hot spot. The theoretical autoignition front propagation speed can thereby be calculated by ξ through [11]

$$u_a^0 = a^0/\xi \tag{4}$$

It is noted that a^0 in Eqs. (2) and (4) is evaluated at initial temperature of T_0=1000 K. However, it is the local sound speed, at the moment when pressure wave passes through, that determines the pressure wave propagation. In order to elucidate such implication, the thermal states of flow particles at different initial locations are tracked [19, 32]. The particle position is updated according to its current flow velocity and its thermal states are obtained through linear interpolation of the corresponding states at its two neighboring grids [19, 32].

Figure 2 shows the evolution of thermal states of flow particles initially located within the hot spot, for a case corresponding to detonation development mode [22, 23] (i.e., PRF100, r_0=5 mm and ξ=3.0, the autoignition process is shown later in Fig. 4). It is seen in Fig. 2(a) that these particles go through three typical stages: (i) an expansion stage characterized by the increase of both specific volume and local pressure (i.e., from the initial state to point A); (ii) a compression stage manifested by a decrease of specific volume and increase of local pressure (i.e. the interval between points A and B). This stage is caused by the propagation of pressure wave induced by earlier autoignition from inner location; and (iii) an

expansion stage after the departure of the pressure wave (i.e. after point B). Figure 2(b) shows that the transient sound speed during the compression stage, a_t>800m/s, is much higher than the initial value of a^0=589 m/s. This is mainly caused by the appreciable increase in local temperature, which reaches above 1600 K at the beginning of the compression stage (see Fig. S4 in the Supplementary Material). Consequently, a_t instead of a^0 should be used to quantify the pressure wave propagation which interacts with local autoignition. Since a_t changes with time, its temporal average during the compression stage, a_c, is calculated. The value of a_c is around 880 m/s for all the particles in Fig. 2 and almost unaffected by their initial locations. This feature is also observed in other cases corresponding to different autoignition modes. Therefore, a_c is used to assess the pressure wave propagation within the hot spot for a specific autoignition case.

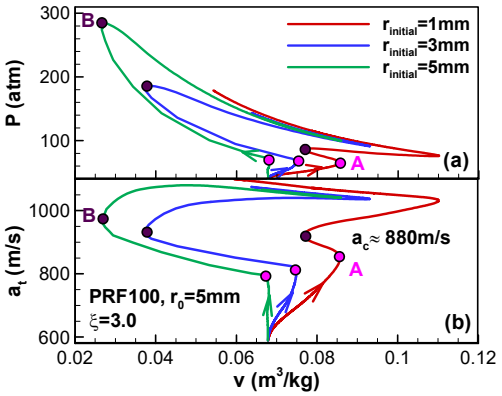

Fig. 2 Change of (a) local pressure and (b) transient sound speed with specific volume for flow particles at different initial positions. The arrows indicate time direction. Points A and B respectively denote the beginning and end of the compression stage caused by the pressure wave propagation.

Figure 3 further shows that that a_c decreases with ξ and r_0, while it increases with c. In fact, the increase of ξ and r_0, and decrease of c (which increases $|(dT/dr)_c|$, see Fig.1) all lead to an increase of the temperature increment of the hot spot core compared with the surrounding mixture (i.e. $T_i(r=0)-T_{i,0}$). Therefore, when ξ or r_0 increases or c decreases, the pressure wave is earlier formed in the hot-spot core (i.e. r=0) and arrives sooner at a given position within the hot spot, when the local temperature is less increased and thus the local sound speed is lower. This leads to a lower value of a_c at higher ξ or r_0, or lower c. For simplicity, a representative value of a_c, i.e. a_r=800 m/s, is proposed to characterize the pressure wave propagation in this study (see Fig. 3). Although the choice of its value is somehow arbitrary, it will be shown later that the utilization of a_r, which is much higher than a^0, helps to accurately capture the fundamental features of chemical-acoustic interactions during autoignition.

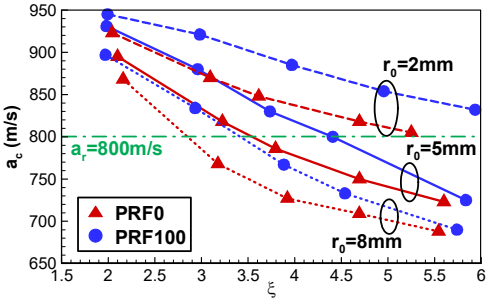

Fig. 3 Change of the averaged sound speed during the compression stage, a_c, with ξ for different PRF compositions and r_0.

Figures 4 shows the change of transient value of spatial maximum pressure, $P_{max,t}$, and the ratio of a_c to the transient autoignition front propagation speed, $u_{a,t}$, with the corresponding location. The autoignition front is defined as the location where T=2200K is achieved. Three autoignition modes are identified [22, 23]: (I) supersonic reaction front propagation for ξ=2.0, (II) detonation development for ξ=3.0, 3.7 and 4.4, and (III) subsonic reaction front propagation for ξ=5.8. The details of pressure evolution in the three detonation cases are similar to those reported in previous studies [22, 23] and thereby are shown in Fig. S5 of the Supplementary Material. Figure 4(b) shows that the autoignition front accelerates during its propagation within the hot spot except for very low value of ξ=2.0. This is mainly due to the non-uniform compression by the pressure wave rather than the heat conduction or mass diffusion, which will be discussed later. When $a_c/u_{a,t}$>1, the pressure wave propagates faster than the autoignition front and the chemical-acoustic interaction is weak. Therefore, the increase in $P_{max,t}$ is rather slow, which is indicated by a low slope in the plot of $P_{max,t}$ versus r in Fig. 4(a). On the other hand, when $a_c/u_{a,t}$≈1, the mutual coupling between local autoignition and pressure wave is greatly enhanced. This initiates a rapid increase of $P_{max,t}$ which corresponds to a much higher slope of the $P_{max,t}$-r curve. Therefore, the incident of $u_{a,t}=a_c$ divides the $P_{max,t}$-r curves into two distinct regimes (see the downward arrows in Fig. 4a), i.e., regime-*W*/regime-*S* with weak/strong chemical-acoustic coupling and slow/rapid pressure increase (i.e. low/high slope of $P_{max,t}$-r curve). It is observed in Fig. 4 that detonation formation usually occurs in the regime-*S*.

Furthermore, two sub-modes of detonation development are identified in Fig. 4: (1) when $u_{a,t}$ approaches a_c at very early stage of autoignition front propagation (e.g. ξ=3.0), regime-*S* dominates and $P_{max,t}$ increases almost linearly with r and a normal detonation development mode (sub-mode II-*N*) is observed; (2) when $u_{a,t}$ approaches a_c at later stage of autoignition front propagation within the hot spot (e.g., ξ=3.7 and 4.4), both regime-*W* and regime-*S* exist, and an over-driven detonation wave is formed (i.e. sub-

mode II-*O*). For sub-mode II-*O*, the peak of $P_{max,t}$ is reached outside the hot spot and it is much higher than that of normal detonation wave. This over-driven detonation mode is mainly attributed to the local autoignition behind the leading pressure/shock wave during the period of $u_{a,t}<a_c$. It leads to local thermal expansion and thereby serves as a hypothetical piston supporting the developing detonation wave to evolve into a strong detonation [33]. However, this temporarily amplified detonation wave is not sustainable and it gradually decays to the level of normal one after reaching its peak pressure (see the curves for ξ=3.7 and 4.4 in Fig. 4a).

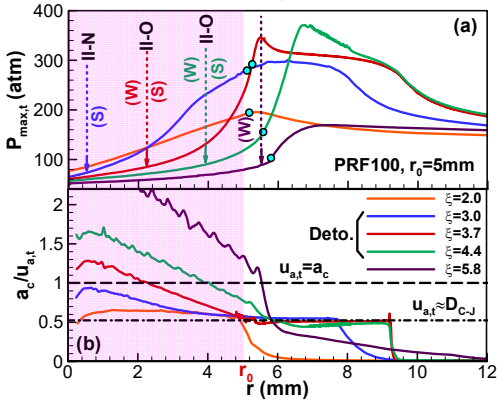

Fig. 4 Change of (a) $P_{max,t}$ and (b) the ratio of a_c to $u_{a,t}$ with the corresponding location, r. The mixture is stoichiometric PRF100/air and the hot spot is indicated by the shadowed area (r_0=5 mm). The downward arrows and circles in Fig. 4(a) respectively indicate the location of $u_{a,t}=a_c$ and the edge of expanding hot spot reached by the autoignition front. The horizontal dash-dotted line in Fig. 4(b) indicates that $u_{a,t}$ approaches C-J detonation wave speed, $D_{C\text{-}J}$=1846 m/s. The values of a_c are: 935 m/s for ξ=2.0, 880 m/s for ξ=3.0, 830 m/s for ξ=3.7, 800 m/s for ξ=4.4, and 725 m/s for ξ=5.8.

Besides, it is noted that a detonation wave (either normal or over-driven type) can be formed only when $u_{a,t}$ approaches a_c well within the hot spot. For the case of ξ=5.8 in Fig. 4, $u_{a,t}$ approaches a_c near the edge of the hot spot, which is too late to initiate an effective chemical-acoustic coupling. Consequently, for ξ=5.8 there is no detonation development.

Unlike the normalized initial temperature gradient, ξ, the following parameter evaluating transient chemical-acoustic interactions, ξ_t, is introduced:

$$\xi_t = a_r / u_{a,spot} \qquad (5)$$

where $u_{a,spot}$ denotes the average speed of autoignition front propagating within the hot spot and is defined as the ratio of hot spot size to the time during which the autoignition front propagates from the hot spot core (i.e. r=0) to its edge. It is noted that ξ_t is different from the counterpart parameter, ξ_a, in our previous work [22, 23] which only considered initial sound speed.

Figure 5 shows the change of the normalized maximum pressure, P_{max}/P_e, with ξ_t and ξ. The value of $P_{max}/P_{v\text{-}N}$ is 0.56 times as that of P_{max}/P_e. It is seen that the peak value of P_{max}/P_e is achieved around ξ_t=1. The slight shift of the peak towards lower ξ_t with decreasing r_0 is mainly due to the fact that a_c increases with decreasing r_0 (see Fig. 3) while only its representative value (i.e. a_r=800 m/s) is used to define ξ_t. Therefore, Fig. 5(a) demonstrates that ξ_t is able to quantitatively assess the intensity of chemical-acoustic interaction and well describe the condition for the formation of the strongest detonation wave (i.e., around ξ_t=1). On the other hand, Fig. 5(b) shows that the value of initial temperature gradient, ξ, corresponding to the peak of P_{max}/P_e is greatly affected by PRF blending ratio and r_0. Therefore, ξ is less suitable for quantitative evaluation of the transient chemical-acoustic interaction during autoignition and detonation development.

Furthermore, Fig. 5 shows that P_{max}/P_e decreases with PRF blending ratio. This is mainly caused by the increase of excitation time, which evaluates the rapidity of ignition heat release, with the blending ratio of iso-octane (see Fig. 1). Besides, higher value of P_{max}/P_e is achieved at larger r_0, obviously due to the longer time provided for the chemical-acoustic coupling within the hot spot.

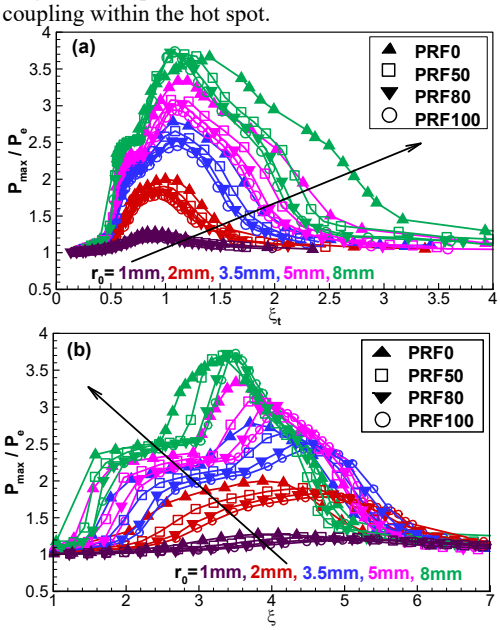

Fig. 5 Change of the maximum pressure in each case, P_{max}, normalized by the equilibrium pressure, P_e, with (a) ξ_t and (b) ξ for different PRF compositions and r_0.

As shown in Fig. 5, a plateau of P_{max}/P_e exists in each curve on the left side of its peak. Figure 6 further plots several specific cases constituting one of the curves in Fig. 5(b) (i.e. PRF100 and r_0=5 mm). It is observed that the P_{max}/P_e plateau is located in the regime of normal detonation development mode (i.e. sub-mode II-*N*). As shown in Fig. 6(b), autoignition in regime II-*N* is characterized by an approximately linear increase of transient spatial maximum pressure with the corresponding location. As ξ further increases, a significant elevation of P_{max}/P_e is

observed on the right side of the plateau (see Fig. 6a), which is located in the regime of over-driven detonation mode (i.e. sub-mode II-*O*). For these cases, the increase of $P_{max,t}/P_e$ with r is strongly non-linear, which consists of both regime-*W* and regime-*S* (also see Fig. 4a). In fact, there is a transition zone between two sub-modes II-*N* and II-*O*. To quantitatively identify these two sub-modes, the right edge of the plateau (e.g. ξ=3.4 in Fig. 6) is chosen as the boundary between them. It is observed that in the case of ξ=3.4 (see the dashed curve in Fig. 6b), the increase of $P_{max,t}/P_e$ with r is actually non-linear and a slightly over-driven detonation wave is formed. However, the peak pressure of this over-driven part is still close to the value of normal detonation wave, which leaves the overall maximum pressure in this case, P_{max}, almost unaffected. When ξ further increases, the over-driven detonation dominates and a significant increment in P_{max} is observed. It is noted that although only results of PRF100 are shown in Figs. 2, 4 and 6, the demonstrated mechanisms and properties of detonation development are essentially similar to those of other PRF compositions.

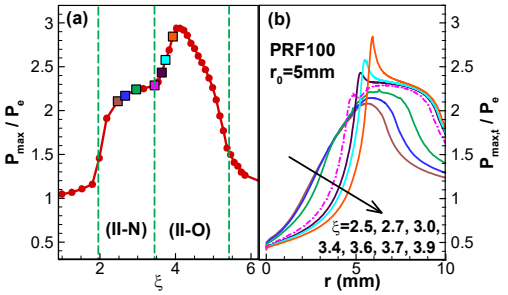

Fig. 6 (a) Change of P_{max}/P_e with ξ in PRF100/air with a hot spot of r_0=5 mm, and (b) change of $P_{max,t}/P_e$ with r in cases denoted by square symbols in Fig. 6(a) with corresponding color.

The effects of PRF composition and hot spot size on autoignition can be assessed by the parameter ε, which is defined as [11]:

$$\varepsilon = r_0 / \left(a^0 \tau_e \right) \tag{6}$$

where τ_e is the excitation time.

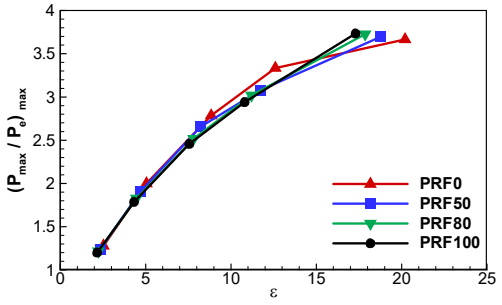

Fig. 7 Maximum value of P_{max}/P_e in each curve in Fig. 5 as a function of ε.

Figure 7 illustrates the influence of ε on the maximum value of P_{max}/P_e. It is observed that all the results for different PRF compositions almost collapse on one curve. This indicates that the parameter ε determines the strength of the strongest detonation initiated by hot spot. Therefore, according to Eq. (6) and Fig. 7, the in-cylinder pressure oscillation and super-knock damages might be mitigated by using reactants with longer excitation time (e.g. through increasing iso-octane ratio in PRF, or applying fuel-lean or diluted conditions [22]) and/or by reducing hot spot size (e.g. through imposing higher turbulence intensity in the cylinder chamber).

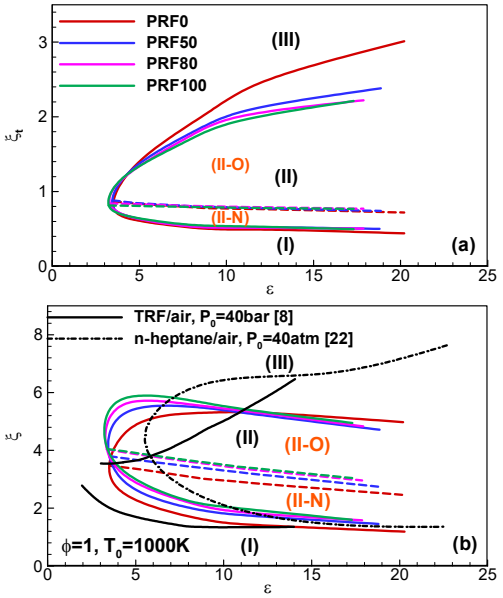

Fig. 8 Regimes of different autoignition modes in the (a) ξ_t-ε and (b) ξ-ε diagrams. These modes include: (I) supersonic reaction front propagation, (II) detonation development consisting of two sub-modes: (II-*N*) normal detonation development and (II-*O*) over-driven detonation development, and (III) subsonic reaction front propagation. The results for TRF consisting of 42.8% isooctane, 13.7% n-heptane and 43.5% toluene [8] and those for n-heptane [22] are also plotted for comparison.

Figure 8 shows the regimes of different autoignition modes in the ξ_t-ε and ξ-ε diagrams. In both diagrams, the detonation regime (II) is bounded by a C-shaped curve, with its two sub-modes, normal and over-driven detonation modes, II-*N* and II-*O*, divided by the dashed lines. In the ξ_t-ε diagram, P_{max}/P_e achieves its maximum value around ξ_t=1 and well within the regime II-*O* (see Figs. S7-S10 of the Supplementary Material). Both the lower and upper limits of the detonation regime expand with ε, indicating that higher ε promotes the detonation propensity, especially that of over-driven detonation. The detonation regimes, especially the normal detonation sub-regimes (II-*N*), agree well with one another for various PRF compositions. On the other hand, in the ξ-ε diagram, notable discrepancies among the detonation regimes, including the sub-regimes, are

observed (the results of TRF/air [8] and n-heptane/air [22] are also plotted for comparison). Furthermore, ξ depicts a much wider (more conservative) detonation regime compared with ξ_t. As shown later, the initial temperature gradient of hot spot, which is assessed by ξ, only partly controls the transient autoignition front propagation. Therefore, the autoignition regimes in ξ-ε diagram are significantly affected by thermal conditions and fuels. On the other hand, according to Figs. 7 and 8, ε gives a satisfactory quantitative prediction of detonation propensity and thereby further refinement of its definition by considering transient sound speed (i.e., a_c or a_r) is not necessary.

Since ξ_t well assesses the transient interaction between local autoignition and pressure wave while ξ can be readily obtained from 0-D calculation, an understanding of the relationship between ξ_t and ξ may be helpful for accurate and efficient prediction of detonation development. Figure 9 shows the change of ξ_t with ξ for all the conditions considered in this study. It is observed that each of the ξ_t-ξ curves consists of two distinctive linear parts with different slopes. These two parts are separated by the boundary between two sub-regimes II-*N* and II-*O*. Besides, ξ_t is much lower than corresponding ξ for all cases, indicating that the transient autoignition front speed is much higher than the theoretical value from 0-D prediction (see Eqs. 4 and 5). A possible cause is the heat conduction and radical mass diffusion during the induction time which may change the spatial distribution of ignition delay. However, by comparing the simulation results with and without considering diffusion terms, it is found that diffusion process has negligible influence on ξ_t, $u_{a,t}$ and P_{max}/P_e for all the autoignition modes examined in this study (see Fig. S11 in the Supplementary Material). This is mainly because the ignition delay under current conditions is too short (i.e., τ<1 ms, see Fig. 1) for the diffusion process to effectively change the temperature and concentration distributions during the induction time. Therefore, the transient autoignition process is hardly affected by the diffusion effect.

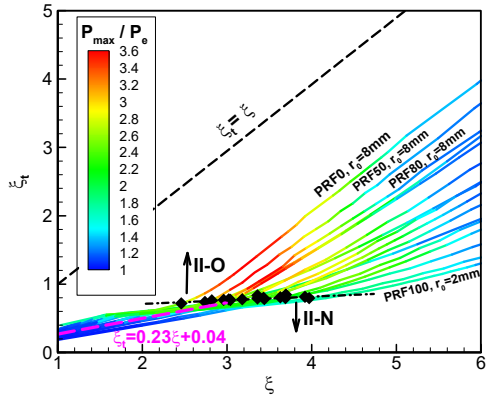

Fig. 9 Change of ξ_t with ξ at different conditions. Each curve represents a specific condition of PRF composition and r_0. The diamond symbols indicate the boundary between the sub-regimes II-*N* and II-*O* in each curve.

In order to reveal the key mechanism causing the deviation of transient autoignition propagation speed from 0-D prediction, Fig. 10 plots the spatial distribution of local ignition delay from 1-D simulation, $\tau_{1\text{-D}}$, and that from 0-D prediction, $\tau_{0\text{-D}}$. The ignition delay here is defined as the time when the local temperature reaches 2200 K and the difference between $\tau_{0\text{-D}}$ and τ is negligible. Figure 10 shows that $\tau_{1\text{-D}}$ is 1.4%-3.5% longer than $\tau_{0\text{-D}}$. Besides, the spatial gradient of $\tau_{1\text{-D}}$ is much shallower than that of $\tau_{0\text{-D}}$, which leads to an appreciably higher transient autoignition front speed compared with the 0-D prediction. By plotting the results simulated without diffusion terms (i.e. the dashed curve), Fig. 10 demonstrates that diffusion has little influence on the $\tau_{1\text{-D}}$ distribution.

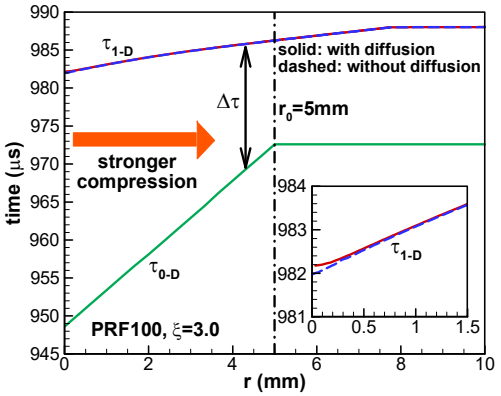

Fig. 10 Spatial distribution of local ignition delay obtained from 1-D simulation and 0-D prediction. For the 1-D simulation, the solid and dashed curves indicate the results with and without diffusion, respectively.

The difference between $\tau_{1\text{-D}}$ and $\tau_{0\text{-D}}$ in Fig. 10 can be interpreted with Fig. 2. In fact, the expansion stage from the initial state to point A in Fig. 2 dominates the induction period of the autoignition process, which constitutes the major portion of the ignition delay (see Fig. S12 in the Supplementary Material). Therefore, $\tau_{1\text{-D}}$ is always longer than $\tau_{0\text{-D}}$ since the latter is obtained in a constant-volume configuration. On the other hand, Fig. 2 shows that both the initial expansion stage and the compression stage (i.e. from point A to B) are affected by the pressure wave propagation. Specifically, the expansion is weakened and the compression is enhanced respectively in these two stages, with the increase of r_{initial}. This is mainly because the pressure wave is continuously strengthened during its propagation within the hot spot (see Fig. 4a). Therefore, the flow particle farther away from the center of the hot spot (i.e. left boundary of the computation domain) is more affected by the compression of the pressure wave, leading to a weakened expansion process and thereby shortened ignition delay at outer location. This non-uniform compression effect makes the difference between $\tau_{1\text{-D}}$ and $\tau_{0\text{-D}}$, i.e. $\Delta\tau=\tau_{1\text{-D}}-\tau_{0\text{-D}}$, decrease with r as shown in Fig. 10. Consequently, $|d\tau_{1\text{-D}}/dr|$ is smaller than $|d\tau_{0\text{-}}$

D/dr|. Therefore, the transient autoignition front propagation speed is much higher than the 0-D prediction, which is manifested by the lower ξ_t compared with ξ as shown in Fig. 9.

The non-uniform compression effect is very prominent in the sub-regime II-*N* due to the continuous enhancement of pressure wave (see the linear increase of $P_{max,t}$ with r in Figs. 4 and 6). This leads to much lower ξ_t compared with ξ below the boundary between sub-regimes II-*N* and II-*O* in Fig. 9. Furthermore, the corresponding parts of ξ_t-ξ curves can be approximated by a linear formula,

$$\xi_t = 0.23\xi + 0.04 \quad (7)$$

with a rather low slope of 0.23.

On the other hand, in the sub-regime II-*O*, the enhancement of pressure wave is weak in the early stage of its propagation (see the non-linear increase of $P_{max,t}$ with r Figs. 4 and 6). This reduces the non-uniform compression effect. Therefore, the autoignition front propagation is less affected and its transient speed approaches closer to the 0-D prediction. As shown in Fig. 9, much higher slope of the ξ_t-ξ curve is achieved in the sub-regime II-*O*. The existence of two distinctive patterns of ξ_t-ξ relationship in sub-regimes II-*N* and II-*O* further demonstrates the major impact of the non-uniform compression effect caused by pressure wave on the transient autoignition process. In comparison, the diffusion effect is negligible since its characteristic time scale is much longer than that of autoignition and pressure wave. Furthermore, it is expected that as long as the autoignition front propagation speed is much higher than the laminar flame speed, the diffusion effect is of secondary importance compared with the compression effect. Otherwise (e.g., extremely high ξ is imposed), the diffusion effect will become important.

4. Conclusions

The 1-D transient autoignition and detonation development induced by a hot spot in PRF/air are studied by simulations considering detailed chemistry and transport. The effects of PRF composition are systematically examined. A new non-dimensional parameter, ξ_t, is introduced to adequately characterize the transient chemical-acoustic interaction and to quantify the autoignition modes. Two detonation sub-modes are identified: normal detonation development (II-*N*) and over-driven detonation development (II-*O*). The maximum pressure caused by autoignition is found to decrease with the blending ratio of iso-octane, mainly due to the increased excitation time. The strongest detonation forms around ξ_t=1 within the sub-regime II-*O* and its maximum pressure is determined by the parameter ε. The deviation of transient autoignition front propagation from 0-D prediction is mainly attributed to the non-uniform compression effect, rather than the diffusion effect including heat conduction and mass diffusion. The former effect is caused by the continuously enhanced pressure wave, which non-uniformly changes the local ignition delay (i.e. reduces its spatial gradient) and accelerates the transient autoignition front propagation. Therefore, ξ_t is always lower than ξ. The relationship between ξ_t and ξ exhibits two patterns with different slopes, which are separated by the boundary between sub-modes II-*N* and II-*O*. This is mainly caused by the different features of pressure wave enhancement in these two sub-modes, which determine the strength of the non-uniform compression effect.

This work is a first step towards a better understanding of autoignition and detonation development in PRF/air mixtures under engine-relevant conditions. In future works, it would be interesting to take into account the influence of thermodynamic conditions [34, 35] and turbulence [24, 25], which might greatly affect the autoignition and detonation development.

Acknowledgements

This work is supported by National Natural Science Foundation of China (Nos. 51976088 and 51861135309) and Shenzhen Sci-Tech Fund (No. JCYJ20210324104802005). We acknowledge the support provided by Center for Computational Science and Engineering at SUSTech.

Supplementary material

A supplementary material associated with this article is provided.

References

[1] Z. Wang, H. Liu, R.D. Reitz, Knocking combustion in spark-ignition engines, *Prog. Energy Combust. Sci.* 61 (2017) 78-112.

[2] G.T. Kalghatgi, D. Bradley, Pre-ignition and 'super-knock' in turbo-charged spark-ignition engines, *Int. J. Engine Res.* 13 (2012) 399-414.

[3] Z. Wang, Y. Qi, X. He, J. Wang, S. Shuai, C.K. Law, Analysis of pre-ignition to super-knock: hotspot-induced deflagration to detonation, *Fuel* 144 (2015) 222-227.

[4] H.Q. Wei, X.J. Zhang, H. Zeng, R. Deiterding, J.Y. Pan, L. Zhou, Mechanism of end-gas autoignition induced by flame-pressure interactions in confined space, *Phys. Fluids* 31 (2019) 076106.

[5] A. Robert, S. Richard, O. Colin, T. Poinsot, LES study of deflagration to detonation mechanisms in a downsized spark ignition engine, *Combust. Flame* 162 (2015) 2788-2807.

[6] H. Wang, M.F. Yao, R.D. Reitz, Development of a Reduced Primary Reference Fuel Mechanism for Internal Combustion Engine Combustion Simulations, *Energy Fuels* 27 (2013) 7843-7853.

[7] M.B. Luong, Z.Y. Luo, T.F. Lu, S.H. Chung, C.S. Yoo, Direct numerical simulations of the ignition of lean primary reference fuel/air mixtures with temperature inhomogeneities, *Combust. Flame* 160 (2013) 2038-2047.

[8] A. Guerouani, A. Robert, J.-M. Zaccardi, Detonation peninsula for TRF-air mixtures: assessment for the analysis of auto-ignition events in spark-ignition engines, *SAE Technical Paper, 2018-01-1721* (2018).
[9] A. Robert, J.-M. Zaccardi, C. Dul, A. Guerouani, J. Rudloff, Numerical study of auto-ignition propagation modes in toluene reference fuel–air mixtures: Toward a better understanding of abnormal combustion in spark-ignition engines, *Int. J. Engine Res.* 19 (2018) 1-12.
[10] D. Bradley, C. Morley, X.J. Gu, D.R. Emerson, Amplified pressure waves during autoignition: relevance to CAI engines, *SAE Technical Paper 2002-01-2868* (2002).
[11] X.J. Gu, D.R. Emerson, D. Bradley, Modes of reaction front propagation from hot spots, *Combust. Flame* 133 (2003) 63-74.
[12] Y.B. Zeldovich, V.B. Librovich, G.M. Makhviladze, G.I. Sivashinsky, On the development of detonation in non-uniformly preheated gas, *Acta Astronaut* 15 (1970) 313-321.
[13] Y.B. Zeldovich, Regime Classification of an Exothermic Reaction with Nonuniform Initial Conditions, *Combust. Flame* 39 (1980) 211-214.
[14] J. Lee, R. Knystautas, N. Yoshikawa, Photochemical initiation of gaseous detonations, *Acta Astronaut* 5 (1978) 971-982.
[15] J. Rudloff, J.M. Zaccardi, S. Richard, J.M. Anderlohr, Analysis of pre-ignition in highly charged SI engines: Emphasis on the auto-ignition mode, *Proc. Combust. Inst.* 34 (2013) 2959-2967.
[16] L. Bates, D. Bradley, Deflagrative, auto-ignitive, and detonative propagation regimes in engines, *Combust. Flame* 175 (2017) 118-122.
[17] R. Lechner, A. Hornung, M. Brautsch, Prediction of the knock propensity of biogenous fuel gases: Application of the detonation theory to syngas blends, *Fuel* 267 (2020) 117243.
[18] J.Y. Pan, S. Dong, H.Q. Wei, T. Li, G.Q. Shu, L. Zhou, Temperature gradient induced detonation development inside and outside a hotspot for different fuels, *Combust. Flame* 205 (2019) 269-277.
[19] P. Dai, Z. Chen, Supersonic reaction front propagation initiated by a hot spot in n-heptane/air mixture with multistage ignition, *Combust. Flame* 162 (2015) 4183-4193.
[20] P. Dai, Z. Chen, S.Y. Chen, Y.G. Ju, Numerical experiments on reaction front propagation in n-heptane/air mixture with temperature gradient, *Proc. Combust. Inst.* 35 (2015) 3045-3052.
[21] T.H. Zhang, W.Q. Sun, L. Wang, Y.G. Ju, Effects of low-temperature chemistry and turbulent transport on knocking formation for stratified dimethyl ether/air mixtures, *Combust. Flame* 200 (2019) 342-353.
[22] P. Dai, Z. Chen, X.H. Gan, Autoignition and detonation development induced by a hot spot in fuel-lean and CO2 diluted n-heptane/air mixtures, *Combust. Flame* 201 (2019) 208-214.
[23] P. Dai, Z. Chen, Effects of NOx addition on autoignition and detonation development in DME/air under engine-relevant conditions, *Proc. Combust. Inst.* 37 (2019) 4813-4820.
[24] M.B. Luong, S. Desai, F.E.H. Perez, R. Sankaran, B. Johansson, H.G. Im, Effects of Turbulence and Temperature Fluctuations on Knock Development in an Ethanol/Air Mixture, *Flow, Turbul. Combust.* 106 (2021) 575-595.
[25] M.B. Luong, S. Desai, F.E.H. Perez, R. Sankaran, B. Johansson, H.G. Im, A statistical analysis of developing knock intensity in a mixture with temperature inhomogeneities, *Proc. Combust. Inst.* 38 (2021) 5781-5789.
[26] P. Dai, Z. Chen, X.H. Gan, M. Liberman, Autoignition and detonation development from a hot spot inside a closed chamber: effects of end wall reflection, *Proc. Combust. Inst.* 38 (2021) 5905-5913.
[27] A. Sow, B.J. Lee, F.E.H. Perez, H.G. Im, Detonation onset in a thermally stratified constant volume reactor, *Proc. Combust. Inst.* 37 (2019) 3529-3536.
[28] H. Yu, Z. Chen, End-gas autoignition and detonation development in a closed chamber, *Combust. Flame* 162 (2015) 4102-4111.
[29] H. Yu, C.K. Qi, Z. Chen, Effects of flame propagation speed and chamber size on end-gas autoignition, *Proc. Combust. Inst.* 36 (2017) 3533-3541.
[30] Z. Chen, M.P. Burke, Y.G. Ju, Effects of Lewis number and ignition energy on the determination of laminar flame speed using propagating spherical flames, *Proc. Combust. Inst.* 32 (2009) 1253-1260.
[31] Z. Chen, Effects of radiation and compression on propagating spherical flames of methane/air mixtures near the lean flammability limit, *Combust. Flame* 157 (2010) 2267-2276.
[32] R. Zhou, J.P. Wang, Numerical investigation of flow particle paths and thermodynamic performance of continuously rotating detonation engines, *Combust. Flame* 159 (2012) 3632-3645.
[33] C.K. Law, Combustion physics, Cambridge Univ Pr, 2006.
[34] Y.L. Qi, Z. Wang, J.X. Wang, X. He, Effects of thermodynamic conditions on the end gas combustion mode associated with engine knock, *Combust. Flame* 162 (2015) 4119-4128.
[35] P. Dai, C.K. Qi, Z. Chen, Effects of initial temperature on autoignition and detonation development in dimethyl ether/air mixtures with temperature gradient, *Proc. Combust. Inst.* 36 (2017) 3643-3650.